

Regeneration Technique for Welding Nanostructured Bainite

K. Fang^a, J. G. Yang^b, X. S. Liu^a, K. J. Song^a, H. Y. Fang^{a,*}, H. K. D. H. Bhadeshia

^c

^a State Key Laboratory of Advanced Welding and Joining, Harbin Institute of Technology, Harbin, 150001, China

^b Institute of Process Equipment and Control Engineering, Zhejiang University of Technology, Hangzhou, 310032, China

^c Department of Materials Science and Metallurgy, University of Cambridge, Pembroke Street, Cambridge CB2 3QZ, U. K.

Abstract

High-carbon steels which are transformed into extremely fine bainite plates embedded in a matrix of carbon-enriched austenite have recently been developed, and have found commercial application in the manufacture of engineering components. However, because of the large carbon concentration, they cannot be welded and this limits the scope for their exploitation. A method is reported here by which the mixture of bainitic ferrite and retained austenite is regenerated to prevent the austenite that is generated by the heat input during welding, from transforming into brittle martensite. The microstructures of the fusion and austenitised zones were characterized by X-ray diffraction, scanning electron microscopes and transmission electron microscopy. Tensile and micro-hardness tests were carried out to evaluate the mechanical properties. The results show

*Corresponding author: Tel: +86-451-86418422; Fax: +86-451-86416186

E-mail: fangkunhit@163.com

that a bead-on-plate weld with the tensile strength of 1850 MPa and the hardness of 600 HV can in principle be achieved; these properties almost match those of the base metal.

Keywords: Nanostructured Bainitic Steel; Welded Joint; Regeneration; Tensile Strength.

1. Introduction

A series of bainitic steels has been developed with an ultimate tensile strength as high as 2.3 GPa and hardness in the range 600-670 HV [1-4]. Both properties are attributed to the fine scale of the carbide-free bainitic ferrite and retained austenite mixture. However, industrial applications of this high-carbon nanostructured bainite are limited because it is difficult to weld [5]; the high carbon concentration (~0.8 wt%) makes it susceptible to cracking in the welded joint due to the formation of brittle, untempered martensite. Hong et al. [6] attempted a rapid post-weld heat treatment to prevent cold cracking by generating a mixture of mildly-tempered martensite and about 40% retained austenite, but unfortunately, the accompanying cementite precipitation ruined the mechanical properties of the joint [7, 8]. Furthermore, the strength of welded joint following the rapid treatment was not as high as that of the base metal.

The ideal scenario would be to obtain fine bainite again after welding, both in the fusion and heat-affected zones. A method called *regeneration* is proposed here to obtain a welded joint with the same microstructure as base metal, so that the mechanical properties do not deteriorate. The regeneration technique is carried out after welding. As the welded joint cools towards the bainite-start temperature B_S , it is transferred into a furnace set at a temperature between B_S and M_S (martensite-start)

and held there to permit the bainite to grow again from any austenite generated during welding process.

2. Experimental procedure

2.1 Materials and experimental procedure

High-carbon ingot steel was austenitised at 1000°C for 20 min, followed by isothermal transformation at 250°C in a furnace for 5 days and finally quenched in water. Its chemical compositions are listed in Table 1. As expected [9, 10], the structure, illustrated in Fig. 1, consists of a mixture of carbide-free bainitic ferrite and carbon-enriched retained austenite.

Plate specimens in dimensions of 2×40×100 mm were machined by spark wire cutting. Bead-on-plate welds with autogenous gas tungsten arc welding were performed along the centerline of these specimens. The welding parameters are listed in Table 2. The specimens for conventional welding were air cooled without heat treatment. Those destined for regeneration were cooled in air, with the temperature of the outer surface monitored using a thermocouple, to ensure they are transferred into the furnace at a temperature just above the regeneration temperature.

2.2 Metallography

The welded joint was sectioned longitudinally and after metallographic preparation, etched using 2% nital. The microstructure was characterised using optical and scanning electron microscopy (Hitachi S-3400N). Foils for transmission electron microscopy (Tecnai G2-F30) observation were thinned to less than 50 µm with emery paper and finished by twin-jet electro-polishing using a solution of 5% perchloric acid in methanol. The volume fraction of retained austenite in the fusion zone was

measured using X-ray diffraction (XRD, D/max-rB) according to the method described in Ref. [11]. Welding specimens were cut off along the joint centreline. After grinding and final polishing using a 2.5 μm diamond paste, an undeformed surface was obtained. Four specimens were put together to achieve a large enough surface. The scanning rate used was 1°/min, at 40 kV and a 40 mA current. The retained austenite content was calculated from the integrated intensities of (200), (220), and (311) austenite peaks, and those of (200), (211), and (220) planes of ferrite. Using three peaks from each phase avoids biasing the results owing to any crystallographic texture in the specimens.

2.3 Mechanical properties testing

The hardness across the weld cross-section was measured using a Vickers's micro-hardness testing machine with a 200 g load. The test lines parallel to the surface of the plate were located at along the centre of the thickness direction. The tensile properties of nanostructured bainitic steel base metal and welded sample following regeneration were tested at room temperature on the Instron-5569 electronic universal experiment machine. Cross-weld test samples with width of 1 mm and thickness of 2 mm for testing area were prepared by spark wire cutting. They were then ground using emery paper to eliminate the effect of welding deformation and surface defect. The elongation was measured by an extensometer with gauge length is 10mm.

3. Results and Discussion

3.1 Design of experimental technique

An approximate assessment of the isothermal transformation kinetics was made using a computer program MAP_STEEL_MUCG46_90 that incorporates the thermodynamics and kinetics of solid-state transformations in steels [12]. The calculated time-temperature transformation (TTT) diagram for the initiation of transformation is shown in Fig. 2, from which it can be seen that bainitic transformation starts at about 300°C, and martensite at 136°C. Using this information, the regeneration temperature was determined to be 250°C, that is, the welded samples after cooling to 300°C, were transferred into a furnace at 250°C and kept there for five days prior to cooling to room temperature.

3.2 Microstructure

Fig. 3 shows the optical microstructure of a conventionally welded joint with the area between the dotted lines subjected to prolonged etching. There are four regions, including the fusion, austenitised and tempered zones, and finally the base metal. According to the chemical compositions and TTT diagram of nanostructured bainitic steel, martensite should be present in both the fusion and austenitised zones, as confirmed by the micrographs in Fig. 4. Cracks can be found, originating from the partially melted zone. Fig. 5 shows the welded joint with regeneration treatment. The fusion and austenitised zones are easy to etch compared to that of conventional welding, while their corrosion degree is similar to base metal, which indicates that the microstructure of fusion and austenitised zones is probably bainite rather than martensite. In addition, it can be seen from Figs 3 and 5 that a lot of black-etching cementite precipitates are observed in tempered zone.

Fig. 6 shows the scanning electron micrographs from the two welds. The fusion zone is composed of a columnar solidification structure. Martensite is apparent in the conventionally welded joint, as shown in Fig. 6c. In contrast, mixed microstructures consisting of film-like bainite and austenite and blocky austenite appear in the fusion zone of the joint with regeneration, as shown in Fig. 6d. The bainite and austenite-films are located mainly in the core of dendrites, while blocky austenite is apparent at the boundaries. Fig. 6e shows the microstructure in the austenitised zone, also consisting of the fine mixture of bainite and austenite. Compared to the microstructure of nanostructured bainite base metal (Fig. 6f), it can be seen from Fig. 6d and Fig. 6e that the apparent thickness of bainite plates increases both in fusion zone and austenitised zone. At the same time the scale of blocky austenite becomes coarser in the fusion zone, and at the dendrite boundaries, presumably because of chemical segregation during solidification. C, Si, Cr and Mn, tend to segregate between dendrite arms, leaving the dendrite cores depleted in these solutes. Table 3 gives the approximate alloy element compositions of the core ('a' in Fig. 6d) and inter-dendritic ('b' in Fig. 6d) regions; carbon is excluded since it is not amenable to analysis using routine energy dispersive X-ray spectroscopy. It can be seen that the alloying element content of the inter-dendritic regions is greater than that in the cores of the dendrites. In this condition, only a small amount of bainite forms between the dendrite arms. On one hand, increasing carbon content will reduce the maximum fraction of bainitic ferrite that can form at the regeneration temperature [13]. On the other hand, increasing alloying elements content will improve the stability of

undercooled austenite [14-17], reduce formation rate of bainite, and then limit the amount of bainitic ferrite during regeneration treatment. Therefore, the austenite in the inter-dendritic regions becomes blocky.

The stability of austenite between dendrite arms in the regenerated weld is surprising, but is understood by the partitioning of carbon from the dendrite cores where bainite forms first [18-20]. As a result, the M_s temperature is reduced to below room temperature, thus stabilising the austenite and avoiding the brittle martensite that forms in the corresponding inter-dendritic regions in the conventional weld.

In order to determine the microstructural evolution after conventional welding and welding with regeneration, the volume fractions of retained austenite were measured by XRD, Fig. 7. For the conventional weld, the ferrite lattice parameter increases because of martensite transformation without carbon diffusion. Therefore, ferrite peaks move to the left and austenite peaks move to the right. The calculated fractions of retained austenite are listed in Table 4. It can be seen that the amount of retained austenite in fusion zone of welded joint with regeneration is a little less than that of nanostructured bainite base metal.

Typical TEM micrographs and corresponding electron diffraction patterns from the fusion zones of the two welds are shown in Fig. 8. It can be seen that the substructure of the martensite in the conventional weld contains twins, while a lath structure is typical in the regenerated joint. Electron diffraction patterns prove that the lath structure is composed of α and γ , i.e. bainitic ferrite and retained austenite.

3.3 Mechanical properties

Fig. 9 shows the distribution of micro-hardness across the welded joints. The fusion and austenitised zones exhibit high hardness in the conventional joint, at about 900 HV. In contrast, for the welded joint with regeneration, the hardness is only about 600 HV in the fusion zone, similar to that of the base metal. It is evident that the regeneration treatment avoids the very large hardness values of the conventionally welded samples.

Fig. 10 shows the stress-strain curves of base metal and the welded joint with regeneration. It can be seen that for nanostructured bainitic steel, the ultimate tensile strength is as high as 1950 MPa and the elongation is about 2%; for welded joint with regeneration, the ultimate tensile strength and elongation are 1410 MPa and 0.8%, respectively. This is much higher than that of conventionally welded joint, which is too low owing to cold cracks formation.

Because in the case of the regenerated joint, fracture occurred in the tempered zone, a tensile test sample containing only the fusion and austenitised zones was prepared, as shown in Fig. 11a. Fig. 11b shows that the fracture takes place in fusion zone, and the ultimate tensile strength is 1852 MPa. This means that the regeneration treatment after welding successfully realises the required bainitic microstructure regeneration in the fusion and austenitised zones, improves their performance, and therefore transfers failure from the fusion and austenitised zone [2, 5, 6] to tempered zone.

Peet [21] has pointed out that the strength and hardness of tempered nanostructured bainite decreased with tempered temperature and time increasing (e.g.

heat input). And it can be seen from Fig. 9 that the hardness of tempered zone decreases with the peak temperature increasing. So, a low heat input during welding should improve the mechanical properties of tempered zone, e.g. the welded joint with regeneration. At the same time, a low heat input will also reduce the width of tempered zone, which potential to further enhance the mechanical properties. Therefore, if regeneration treatment is used in combination with a low heat input welding method, such as laser welding, it may lead to a further optimisation of the mechanical properties of the welded joint in base metal that is nanostructured bainite.

4. Conclusions

Microscopic cracks are easily found in conventionally welded joints of nanostructured bainitic steel because of the generation of untempered, high-carbon and brittle martensite due to the heat input from the welding operation. A regenerating heat treatment has been designed to avoid this cracking. The weld, before it cools below 300°C, is transferred into a furnace at 250°C in order to allow any regions that become austenite at high temperatures, to transform into bainite of a similar form to the original base metal. This dramatically reduces the tendency for cracking and the tensile properties obtained for the fusion and reaustenitised regions are promising.

One further problem remains, that the tempered region in the heat affected zone of the welded joint becomes the point of failure in cross-weld tensile tests. It is suggested that further experiments involving low heat input welding may mitigate this issue.

Acknowledgement

The authors are grateful to Steve Ooi for the helpful discussions on microstructure analysis and Mathew Peet for his research on tempering of low-temperature bainite.

References

- [1] Caballero FG, Bhadeshia HKDH. Very strong bainite[J]. *Current Opinion in Solid State and Materials Science* 2004;8:251-257.
- [2] Bhadeshia HKDH. Nanostructured bainite. *Proceedings of the Royal Society A* 2010;466:3–18.
- [3] Garcia-Mateo C, Caballero FG, Bhadeshia HKDH. Low temperature bainite. *Journal de Physique IV* 2003;112:285–288.
- [4] Bhadeshia HKDH. Properties of fine-grained steels generated by displacive transformation. *Materials Science and Engineering A* 2008;481:36–39.
- [5] Fang K, Yang JG, Fang HY. Review of nanobainite steel welding. *Advanced Materials Research* 2012;482-484:2405-2408.
- [6] Hong SG: Effects of post weld rapid heat treatment on microstructural evolution in high-carbon bainitic steel weld, in: 63rd Annual Assembly & International Conference of the International Institute of Welding, Istanbul, Turkey, 11-17 July, 2010.
- [7] Zhang YD, Esling C, Calcagnotto M, Gong ML, Zhao X, Zuo L. Shift of the eutectoid point in the Fe–C binary system by a high magnetic field. *Journal of Physics D: Applied Physics* 2007;40(21):6501-6506.
- [8] Ohmori Y, Tamura I. Epsilon carbide precipitation during tempering of plain

- carbon martensite. Metallurgical and Materials Transactions A 1992;23(10):2737-2751.
- [9] Hase K, Garcia-Mateo C, Bhadeshia HKDH. Bimodal size-distribution of bainite plates. Materials Science and Engineering A 2006;438-440:145-148.
- [10] Yoozbashi MN, Yazdani S, Wang TS. Design of a new nanostructured, high-Si bainitic steel with lower cost production. Materials and Design 2011;32:3248–3253.
- [11] Yang J, Wang TS, Zhang B, Zhang FC. Microstructure and mechanical properties of high-carbon Si–Al-rich steel by low-temperature austempering. Materials and Design 2012;35:170–174.
- [12] Bhadeshia HKDH. Thermodynamic analysis of isothermal transformation diagrams. Metal Science 1982;16:159-165.
- [13] Matsuda H, Bhadeshia H K D H. Kinetics of the bainite transformation. Proceedings of the Royal Society A. 2004;460: 1707–1722.
- [14] Chang LC. Bainite transformation temperatures in high-silicon steels. Metallurgical and Materials Transactions A 1999;30(4):909-916.
- [15] Gibbs PJ, Moor ED, Merwin MJ, Clausen B, Speer JG, Matlock DK. Austenite stability effects on tensile behavior of manganese-enriched-austenite transformation-induced plasticity steel. Metallurgical and Materials Transactions A 2011;42(12):3691-3702.
- [16] Matsuo TT, Kasama AH, Kiminami CS, Botta WJ, Bolfarini C. Retained austenite in spray formed high chromium white cast iron. Journal of Metastable

and Nanocrystalline Materials 2004;20-21:397-302.

- [17] Hanzaki AZ, Hodgson PD, Yue S. Retained austenite characteristics in thermomechanically processed si-mn transformation-induced plasticity steels. Metallurgical and Materials Transactions A 1997;28(11):2405-2414.
- [18] Avishan B, Yazdani S, Nedjad SH. Toughness variations in nanostructured bainitic steels. Materials Science and Engineering A 2012;548(30):106–111.
- [19] Caballero FG, Bhadeshia HKDH, Mawella KJA, Jones DG, Brown P. Very strong low temperature bainite. Materials Science and Technology 2002;18:279-284.
- [20] Amey CM, Huang H, Rivera-Díaz-del-Castillo PEJ. Distortion in 100Cr6 and nanostructured bainite. Materials and Design 2012;35:66–71.
- [21] M. J. Peet: Transformation and tempering of low-temperature bainite. Doctor Thesis·University of Cambridge 2010.

Figure captions

Fig.1. Transmission electron micrograph of nanostructured bainite

Fig.2. Calculated time-temperature-transformation diagram, 'P' stands for pearlite

Fig.3. Conventionally welded joint

Fig.4. Cracks in conventionally welded joint

Fig.5. Welded joint with regeneration

Fig.6. Scanning electron micrographs of (a) fusion zone of conventional welding joint, (b) fusion zone of welded joint with regeneration, (c) magnified views of the regions in (a), (d) magnified views of the regions in (b), (e) austenitised zone of welded joint with regeneration, (f) nanostructured bainitic steel

Fig.7. XRD patterns of nanostructured bainite base metal and weld metal of two welded joints

Fig.8. Typical TEM micrographs and electron diffraction patterns in fusion zone of (a) conventionally welded joint, (b) welded joint by regeneration

Fig.9. Plot of hardness values as function of distance to centreline of weld

Fig.10. Stress-strain curves by tensile test

Fig.11. Tensile test sample for fusion and austenitised zones with regeneration (a) before stretching, (b) after stretching

Tables

Table 1 Chemical compositions of the steel (wt%)

Element	C	Si	Cr	Mn	Al	S	P	V	Fe
Wt%	0.76	1.63	1.31	1.04	0.01	0.003	0.008	0.1	balance

Table 2 Welding parameters

Welding Current	Welding Voltage	Welding Speed	Shielding Gas Flow (Argon)
140A	20V	185 mm/min	7.5 L/min

Table 3 The alloying elements compositions of the solute-depleted and solute-enriched regions (wt%)

	Si	Cr	Mn
a	2.07	1.41	1.37
b	2.56	2.17	1.92

Table 4 The calculated fractions of retained austenite of nanostructured bainite base metal and the two welds

	Welded joint with regeneration	Conventionally welded joint	Nanostructured bainite base metal
V_{γ} , %	17.59	16.99	19.12

Figures

Fig.1

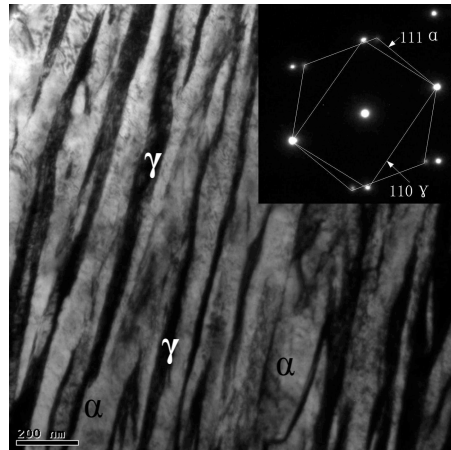


Fig.2

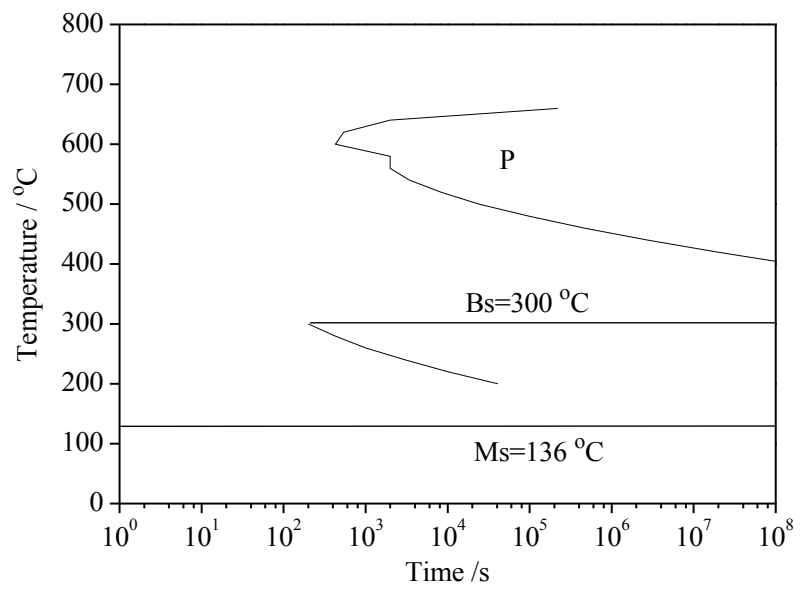


Fig.3

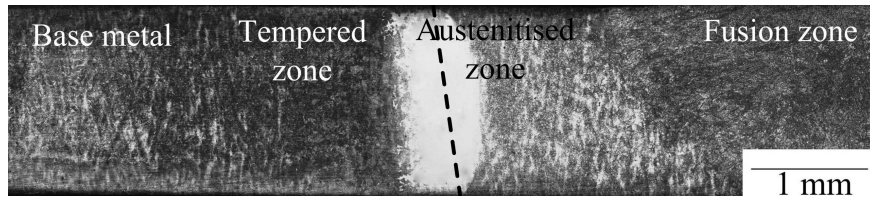


Fig.4

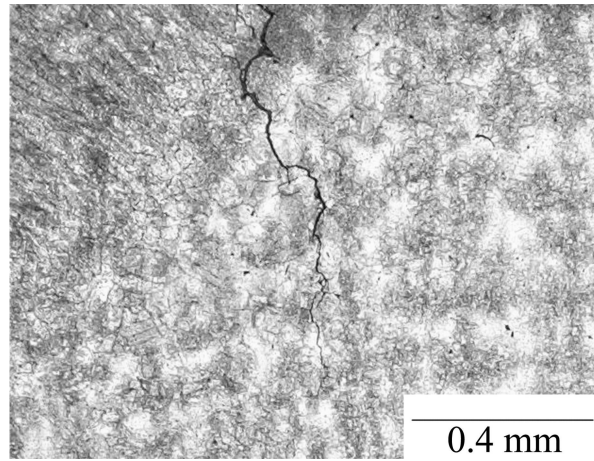
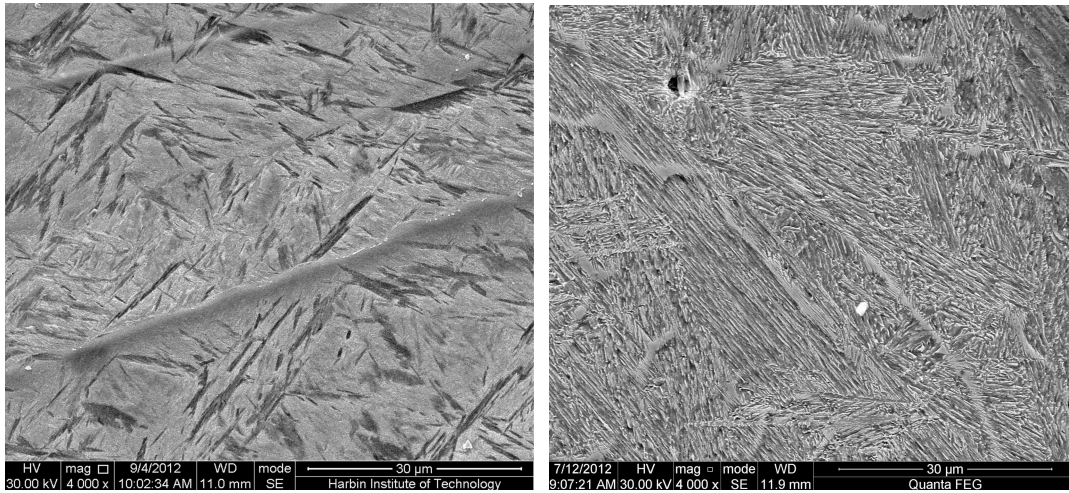


Fig.5

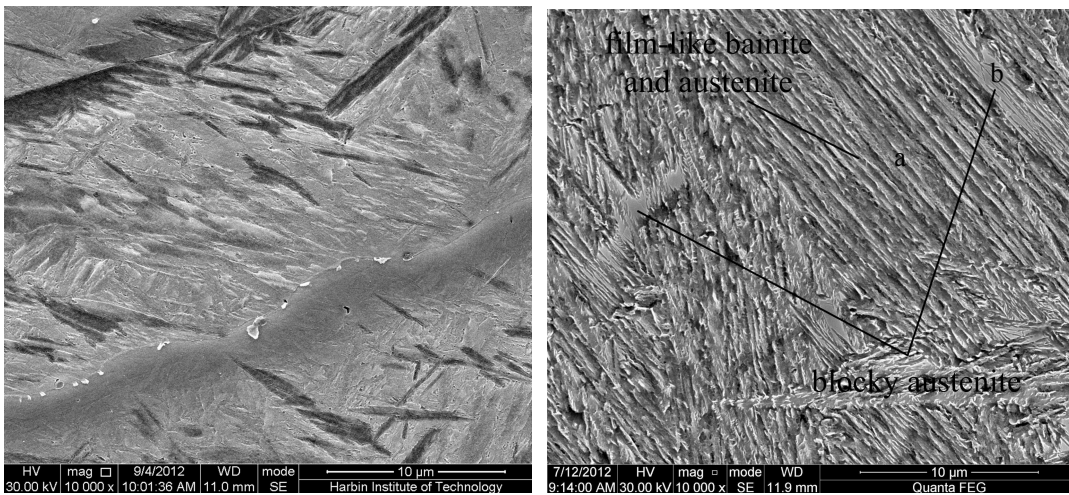


Fig.6



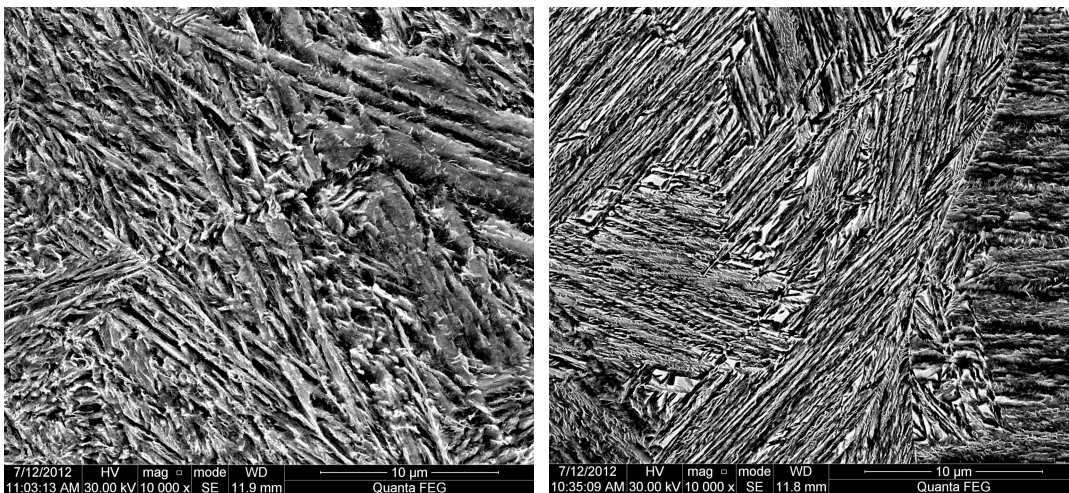
(a)

(b)



(c)

(d)



(e)

(f)

Fig.7

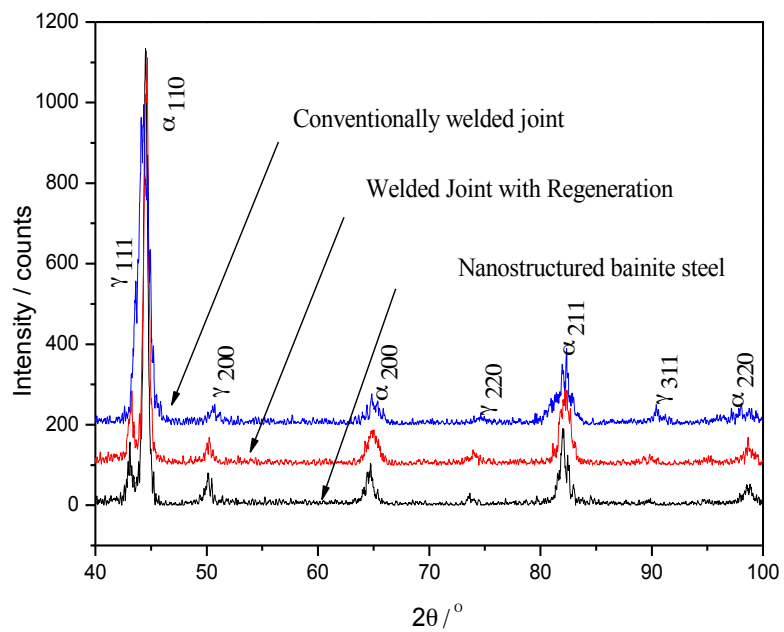


Fig.8

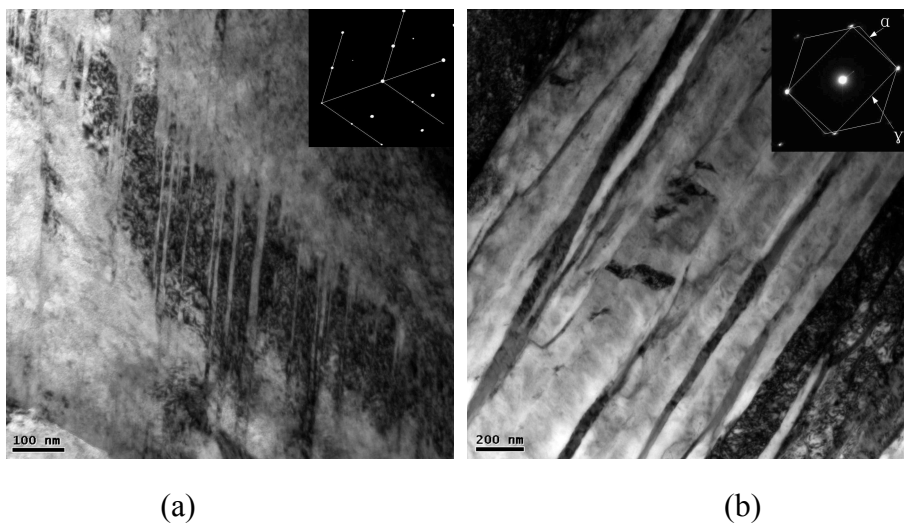


Fig.9

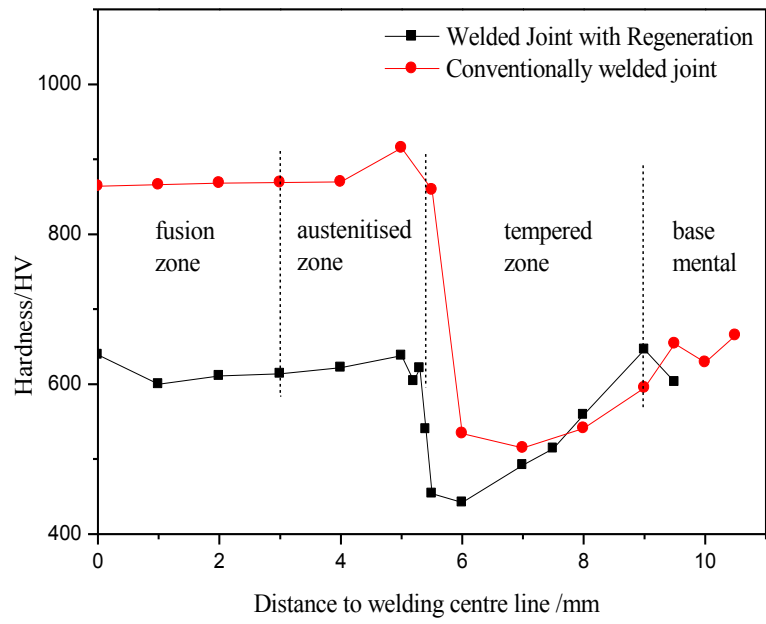


Fig.10

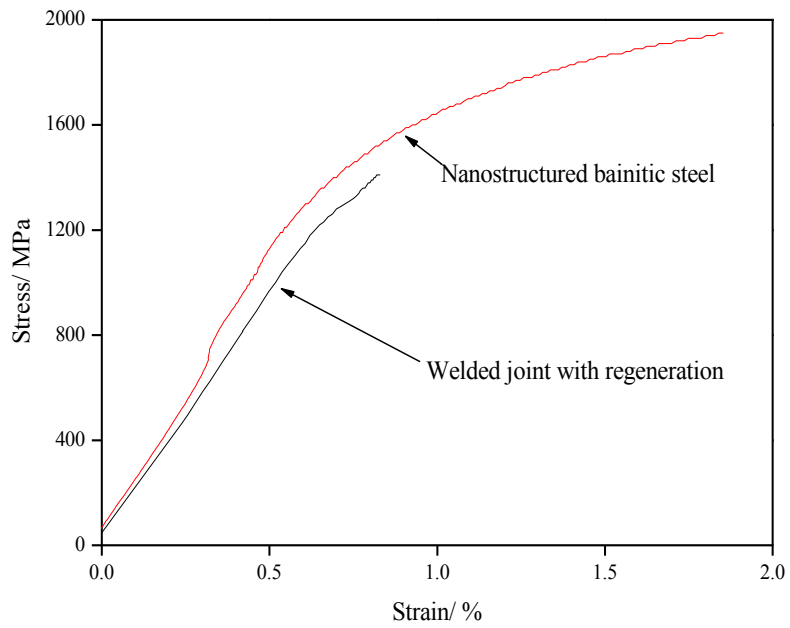


Fig.11

